scientific reports

Check for updates

OPEN

Multiple cell types including melanocytes contribute to elastogenesis in the developing murine aortic valve

Sana Nasim[1], Beatriz Abdo Abujamra[3], Daniel Chaparro[1], Perony Da Silva Nogueira[2,3], Alberto Riva[4], Joshua D. Hutcheson[1,2,5]✉ & Lidia Kos[2,3,5]✉

Elastic fibers are crucial for aortic valve (AoV) function and are generated and maintained by valvular interstitial cells (VICs). VICs exhibit diverse phenotypes, yet the specific subpopulation responsible for producing and regulating elastic fibers remains unclear. This gap in knowledge is significant, given that elastin (Eln) abnormalities lead to congenital AoV defects and initiate AoV diseases. This study characterizes the timing of *Eln* expression in murine AoV, revealing it peaks during late embryogenesis and early postnatal stages, decreasing in adulthood. Spatial transcriptomics and RT-qPCR indicate that *Eln* expression correlates with genes associated to elastogenesis, including *Acta2*, a smooth muscle cell marker. While *Eln* expression is not exclusive to a single VIC subpopulation, RNAscope and immunofluorescence demonstrate a population of *Eln*-expressing VICs that co-express alpha smooth muscle actin and melanocytic markers. As previously reported in adult mice, we show a relationship between AoV pigment and elastic fiber patterning during early postnatal stages and further show that melanocytes may play a critical role in elastogenesis. In summary, *Eln* is expressed in the AoV during early postnatal stages by cells co-expressing markers of various types, highlighting the complexity of VICs phenotypes and their role in elastic fiber regulation.

Elastogenesis is a complex process that involves the precise interaction of several proteins regulated in a spatiotemporal manner to produce mature elastic fibers. These fibers store and release elastic energy in blood vessels and heart valves over the course of the cardiac cycle[1]. In the skin, elastin (Eln), along with collagen, maintains skin elasticity and supports tissue structure[2]. In the lungs, elastin facilitates expansion and contraction over one billion events in an average human lifetime, which is necessary for respiration[3,4]. Elastogenesis occurs mostly during fetal and early stages of organ development. In the murine aorta, *Eln* expression and protein synthesis occur within a narrow timeframe of embryonic (E) stage 14 to postnatal (P) stage 21[5].

In the semilunar valves (aortic valve (AoV) and pulmonary valve), the layer facing the ventricle is mainly composed of an organized elastic fiber network, which is essential for proper physiological function[6,7]. *Eln* null mice die at birth and *Eln* haploinsufficiency (Eln $^{+/-}$) results in decreased aortic diameter with increased structural stiffness leading to increased blood pressure over time[8–10]. In humans, *Eln* mutations correlate with bicuspid AoV disease[11]. Additionally, Eln degradation has been implicated as an important initiation event in AoV remodeling leading to calcification[12]. Despite the critical relevance of elastic fibers in AoV biomechanics and disease, little is known about the cellular-level mechanisms leading to elastogenesis in AoV development, and previous single cell-based analyses have been unable to positively identify specific AoV cellular subpopulations responsible for Eln expression[13].

During embryogenesis, two major cell lineages – endocardial and neural crest (NC), contribute to the formation of the semilunar valves. Recent studies have indicated that a third lineage, cells from the second heart field, also participates in the formation of semilunar valves[14,15]. These developmental lineages give rise to the two major valvular cell types, valvular endothelial cells (VECs) and valvular interstitial cells (VICs). In mice, the AoV is pigmented and contains cells that express melanocytic markers such as Microphthalmia-associated Transcription Factor (Mitf), dopachrome tautomerase (Dct), Tyrosinase related protein 1 (Trp1) and Tyrosinase (Tyr). As early as E12.5 in the developing murine heart, cells that express Dct have been observed in

[1]Department of Biomedical Engineering, Florida International University, Miami, FL 33174, USA. [2]Biomolecular Sciences Institute, Florida International University, Miami, FL 33199, USA. [3]Department of Biological Sciences, Florida International University, Miami, FL 33199, USA. [4]Human Technopole, Milan 20157, Italy. [5]These authors contributed equally: Joshua D. Hutcheson and Lidia Kos . ✉email: jhutches@fiu.edu; kosl@fiu.edu

the atrioventricular (AV) valves. The migration of these cells depends on Kit and endothelin receptor b signaling, suggesting a NC origin similar to skin melanocytes[16]. These cells have also been shown to contribute to valve stiffness and extracellular matrix patterning. We have recently shown a relationship between pigmentation and elastic fiber patterning using two-photon imaging and wholemount confocal microscopy in the murine AoV[17,18]. Hyperpigmentation is associated with disrupted elastic fiber patterning, while hypopigmentation associates with lack of elastic fibers in the AoV. Though our previous reports demonstrate clear AoV elastic fiber phenotypes in correlation with altered pigmentation, it remains unclear whether cells that express melanocytic markers express *Eln* directly or control elastogenesis through paracrine signaling to other cellular populations in the AoV.

Here, we explore the timeline of Eln production in the AoV during development. Moreover, we explore AoV elastic fiber patterning during early postnatal stages as well as the cellular phenotypes responsible for *Eln* production. Using wholemount confocal microscopy and RNAscope in situ hybridization, we demonstrate that *Eln* is produced by multiple cell types, such as endothelial cells, interstitial cells, and smooth muscle cells. Interestingly, we found a population of *Eln* producing cells to have a unique phenotype that co-expresses smooth muscle cell and melanocytic markers.

Materials and methods

Transgenic animals and genotyping

All mice were housed in the Florida International University Animal Care Facility. The animal protocol for this study was approved by the Institutional Animal Care and Use Committee (IACUC 19 – 017). IACUC regulations were followed throughout the study. All methods were performed in accordance with the relevant guidelines and regulations. All methods are reported in accordance with ARRIVE guidelines when appropriate. C57BL/6J wild type mice (WT for simplicity; Stock number 000664), and B6(Cg)-Tyr$^{c-2\,J}$/J mice (Albino for simplicity; stock number: 000058) were purchased from Jackson Laboratory (Bar Habor, ME). The K5-tTA; TRE-Edn3-lacZ (K5-Edn3, for simplicity) transgenic mice were generated in our laboratory[19].

Genomic DNA was isolated from postnatal pups and adult mice tail biopsies. Genotyping of K5-Edn3 mice was performed using the primers 5' CCAGGTGGAGTCACAGGATT 3', 5' ACAGAGACTGTGGACCACCC 3', for the recognition of the K5-tTA gene and, 5' GGCCTGTGCACACTTCTGT 3', 5' TCCTTGTGAAACTGGAG CCT 3' for the TRE-Edn3-LacZ transgene. Routine PCR conditions were used (35 cycles of 94 °C for 30 s, 60 °C for 60 s, and 72 °C for 60 s) with an initial 3 min hold at 94 °C. PCR product was then visualized in 1.5% agarose gel containing 0.5ug/ml ethidium bromide (Thermo Fisher Scientific, Pittsburgh, PA). The K5-tTA produced a 244 bp product whereas the TRE-Edn3-LacZ produced a 463 bp band.

Reverse transcription-quantitative polymerase chain reaction (RT-qPCR)

Hearts were freshly resected from different stages of embryonic and postnatal mice after euthanasia via decapitation. All tissue dissections were performed on ice. AoV were isolated and snap frozen in -80 °C until all samples ready for RNA isolation. Total RNA was isolated using GeneJET RNA Purification Kit according to the manufacturer's protocol (Thermo Fisher Scientific, Pittsburgh, PA, Cat# K0731) and was eluted in 15 µl nuclease-free water. Isolated RNA quantity and concentration were verified using a NanoDrop 2000c spectrophotometer (Thermo Fisher Scientific, Pittsburgh, PA). 50ng of total RNA was used for the reverse transcription using the Maxima first-strand cDNA synthesis kit (Thermo Fisher Scientific, Pittsburgh, PA, Cat# K1642). The cDNA was synthesized using the Oligo $(dT)_{15}$ primer according to the manufacturer's protocol (temperature cycles: 5 min for 25 °C and 60 min for 42 °C and 5 min for 85 °C). RT-qPCR was performed using a commercially available Maxima SYBR Green/ROX qPCR Master Mix (Thermo Fisher Scientific, Pittsburgh, PA, Cat# K0251). Signals were detected using a Step-One Real-Time PCR System (Applied Biosystems, Grand Island, NY). In brief, the PCR tubes (Applied Biosystems, Waltham, MA) were incubated at 95 °C for 10 min before initiating the cycle for Taq polymerase activation. The cycling parameters were as follows: 95 °C for 15 s; 58 °C for 60 s. Finally, the change in cycle threshold (ΔCt) values were averaged and normalized with Gapdh, an endogenous housekeeping gene. $2^{-\Delta Ct}$ method was used to express relative gene expression for the various embryonic time points. All the primer sequences are listed in Supplemental Table S1.

Spatial transcriptomics

Aortic Valve Dissections – Hearts were freshly resected from P3 mice ($N=4$) after euthanasia via decapitation. All tissue dissections were done on ice. A transverse cut was made to remove the apex of the heart. Atria, pulmonary artery, and right ventricle were carefully resected. Finally, the remaining posterior aspect of the left ventricle and mitral valve were removed. The remaining tissue (interventricular septum, anterior aspect of left ventricle and mitral valve, AoV, and aortic root) were snap frozen in a liquid nitrogen cooled bath of isopentane. The tissues were then embedded in 7 × 5 × 5 mm disposable base molds in OCT ensuring that the long axis of the tissue was perpendicular to one of the mold faces and then stored at -80°C.

Sectioning, Staining, Imaging– Tissue molds were placed in a cryostat at -20 °C for sectioning. Molds were cut proximal to the tissue to prevent OCT overlap within a capture area of the 10X Visium Spatial slides (10X Genomics, Pleasanton, CA). Serial caudal transverse sections of the tissue were made starting from the superior aspect of the aortic root and placed on microscope slides to determine when the AoV was reached. Once at the AoV, serial 16 µm sections of tissue were placed on the 10X Genomics Visium Spatial slides. Two to six consecutive sections were placed on a single capture area. Two capture areas were used for each biological sample. We followed 10x Genomics "Methanol Fixation, H&E Staining and Imaging - Visium Spatial Protocols" protocol (CG000160) to fix and stain the tissues on the slides. A Zeiss Axio Observer.Z1 microscope was used to create large, high resolution (0.91 µm/pixel), stitched images of the capture areas ensuring the fiducial frame of each capture area was clearly visible (Supplemental Fig. 1).

Library Construction and Sequencing – For the library construction, 25% of the total cDNA samples obtained from the capture areas were used. cDNA was eluted with buffer EB, followed by fragmentation and adaptor ligation. Post ligation cleanup using SPRIselect (Beckman Coulter Cat# B23317), PCR-based sample indexing, and quality analysis using Agilent bioanalyzer high sensitivity chip were performed. Illumina NovaSeq6000 platform was used with 25 million reads per area. Sequencing was done on S4 flow cell lanes using 300 cycles.

Data Analysis –We used 10X Genomics Loupe Browser visualization software to manually select the AoV leaflet tissues within the tissue sections. Log2 fold change up-regulated differential expression between AoV leaflet and surrounding tissues was done with the built in Loupe Browser (Supplemental Table S2). The corresponding barcodes to the manually selected spots corresponding to the AoV leaflet tissue were imported into MATLAB for subsequent analysis. A custom MATLAB script was used to align the raw read count data set with the spatially identified AoV leaflet barcoded spots. For each spot (131 total), gene read count values were normalized to the total number of reads for a given spot. Unbiased correlation of *Eln* expression with every other expressed gene per spot was done using the corrcoef built in MATLAB function. Only spots with non-zero read counts per gene were used in the analysis. (Supplemental Table S3).

Cryosection immunofluorescence

AoVs were fixed in 4% paraformaldehyde (PFA) for 30 min at room temperature and subjected to serial sucrose incubation of 10% and 20% overnight at 4 °C. Tissues were then embedded in OCT and kept at -80 °C. 7–10 µm thick cryosections were cut using a cryostat (CM3050S, Leica) and kept at -80 °C until further staining steps. Before use, slides were thawed for 5 min and dried at 60 °C for an hour. Pigment bleaching was performed by incubating the slides in 10% H_2O_2 overnight in 1X PBS. Sections were incubated in blocking buffer (10% goat serum, 0.3% Triton X-100, 1% BSA) at room temperature for 1 h followed by primary antibody incubation at room temperature for 1 h or at 4 °C overnight. The primary antibody was diluted in a buffer containing 1% goat serum, 0.3% TritonX-100, and 1% BSA. Sections were thoroughly washed before incubating in secondary antibody for 1 h at room temperature. All primary and secondary antibodies used in this study are listed in Supplemental Table S4. Before sealing the slide with fluoroshield mounting medium with DAPI, slides were thoroughly washed with 1X PBS. Images were taken on an Olympus Confocal BX61 microscope.

Wholemount immunofluorescence

AoVs were harvested from mouse hearts and fixed in 4% PFA for 30 min at room temperature and washed in 1X PBS twice. Tissues were then pigment bleached using 10% H_2O_2 overnight in PBS. Light microscope images were taken before pigment bleach. Tissues were then washed with 1X PBS and processed for wholemount antibody staining. In brief, tissues were permeabilized in 1% Triton X-100 in PBS for 45 min, blocked (10% goat serum, 0.3% Triton X-100, and 1% bovine serum albumin (BSA)) for 2 h at room temperature on a shaker followed by primary antibody incubation at 4 °C overnight on a shaker. The primary antibody was diluted in a buffer containing 1% goat serum, 0.3% TritonX-100, and 1% BSA. Tissues were thoroughly washed for 2 h with 1X PBS at room temperature, before secondary antibody staining for 1.5 h. Lastly, tissues were washed for 2 h with 1X PBS at room temperature and incubated in DAPI for 2 min and mounted with a mounting medium. The AoV cusps were positioned such that the AoV faced upward as z-stack images were obtained using an upright Olympus Confocal BX61 microscope. All z-stacks were 3-D reconstructed using NIH ImageJ.

RNAscope *in situ* hybridization

RNAscope (Advanced Cell Diagnostics, Newark, CA) combined with immunofluorescence was used to assess *Eln* or *Tyr* mRNA with alpha smooth muscle actin (αSMA), Trp1, CD45, and VE-Cad antibody staining. All primary antibodies dilutions are listed in Supplemental Table S4. In brief, wholemount AoV tissue samples, or sectioned slides (7 µm) were exposed to sequential ethanol dehydration, brief hydrogen peroxide treatment, target retrieval treatment leading to protease treatment, and probe hybridization (Advanced Cell Diagnostics; Mm-Eln-C1 Cat#319361 and Mm-Tyr-C2 Cat#422491) for 2.5 h. Tissues were kept in 5X saline sodium citrate buffer overnight until further processing. Probe amplification steps for *Eln* HRP channels were developed for each mRNA channel separately. Once the RNAscope steps were completed, tissues were fixed in 4% PFA for 15 min before proceeding to routine immunofluorescence steps discussed previously in the immunofluorescence section.

Structural imaging and quantification

Alexa Fluor 633 (AF 633) hydrazide (Thermo Fisher Scientific, Pittsburgh, PA, Cat#A30634) was used for elastic fiber staining as previously described[17,20,21]. 0.2 µM AF633 probe in PBS was used along with 10 µM CNA35-488 for collagen fiber staining (kindly gifted by Chris Reutelingsperger from Maastricht University, Netherlands)[22]. Wholemount AoV tissue staining was carried for 45 min incubation at room temperature before 4% PFA fixation followed by pigment bleaching in 10% H_2O_2 overnight. Tissues were then placed on a glass slide with the three cusps of the AoV facing up and sealed with a coverslip. Z-stack images were taken using an Olympus Confocal BX61 microscope. 3-D reconstruction and quantification were done with Fiji (https://imagej.nih.gov/ij/) using the 3-D viewer plugin and ROI Manager, respectively[23].

Statistical analysis

All quantitative data are given as mean ± standard error mean. 'N' indicates the number of biological replicates and 'n' indicates the number of technical replicates. Statistical packages in GraphPad Prism 9 were utilized for data normality and variance between the groups. Statistical differences were determined either by a t-test or one-way ANOVA along with Tukey's post hoc multiple comparison test with significance considered as $p < 0.05$.

Results

Aortic valve *eln* expression peaks in early postnatal stages

To assess the timeline of *Eln* expression, murine WT AoVs were isolated from various embryonic stages beginning from E13.5 to postnatal stages up to adulthood (12–13 weeks old). *Eln* expression remains low during early embryogenesis (E13.5 to E16.5) and increases 5-fold ($p < 0.0001$) during late embryogenesis (E17.5 and E18). Through early postnatal stages (P0-P5), *Eln* expression continues to increase 12–28 fold before returning to low levels in adulthood (Fig. 1). These results indicate that *Eln* gene expression is limited to a short time immediately before and after birth.

Spatial transcriptomics reveals correlation of elastin with known elastogenesis genes

At P3, using spatial transcriptomic analysis we found that valve tissue could be separated from other surrounding cardiac tissue based on global gene expression patterns (Fig. 2A and B). A list of all statistically significant up-regulated differentially expressed genes in the AoV leaflet tissues compared to the surrounding tissues can be seen in Supplemental Table S2 sorted by ascending p-value.

Unbiased analysis of *Eln* correlation to other genes resulted in 369 statistically significant ($P < 0.05$) genes positively correlated with *Eln* expression. Of these genes, 3 had a "very strong" correlation ($0.8 < R < 1$), 36 had a "moderate" correlation ($0.6 < R < 0.8$), 119 had a "fair" correlation ($0.3 < R < 0.6$), and 26 had a "poor" correlation ($0 < R < 0.3$) using Akoglu (2018) User's guide to correlation coefficients[24] and further adapted[25]. The list of genes, their correlation coefficient to *Eln* expression, and their corresponding p-value are in Supplemental Table S3 sorted by ascending p-value. The top ten correlated genes, (Fig. 2C), includes *Fbln5*, *Lox*, and *Fn1*, which are known key regulators of elastic fiber formation in the aorta[26–28]. The most correlated gene was *Acta2*, a common marker of smooth muscle cells and myofibroblasts, cell types previously reported to mediate elastogenesis.

Eln is expressed in alpha-smooth muscle actin positive cells

To further test the relationship between Eln production and αSMA positive cells in the WT AoV, in situ hybridization using RNAscope combined with immunofluorescence were performed. P0 AoVs were assessed due to the noted increase in *Eln* in early postnatal stages (Fig. 1A). In tissues other than heart valves, fibroblasts and smooth muscle cells are known to be responsible for elastogenesis[29,30]. We found that cells expressing αSMA expressed *Eln* in the AoV at P0 stage (Fig. 2D).

Murine hypopigmentation associates with less fibers in early postnatal development

We previously showed that AoV elastic fiber patterning is altered in adult mice with different pigmentation phenotypes, where the AoVs of hyperpigmented (K5-Edn3) mice have disrupted elastic fibers and AoVs from hypopigmented (Kit^{Wv} and Albino) mice are largely devoid of elastic fibers[17,18]. The K5-Edn3 transgenic mice express the cytokine endothelin 3 (End3) under the control of keratin promoter leading to excess pigmentation in cutaneous and non-cutaneous sites[19]. The Albino mice contain melanocytes but melanogenesis is blocked by a mutation in Tyr, which is a pigment rate limiting enzyme. Here, we investigated early postnatal stages to assess the timing of changes in the extracellular matrix fiber patterning that occurs with the variation of pigment. To assess the structural patterning of Eln and collagen, AF633 and CNA35-488, respectively, were used in wholemount AoVs at P0 and P7 stages (Supplemental Fig. 2). In WT P0, qualitative observations indicated that elastic fibers were circumferentially aligned with collagen fibers, whereas at P7 elastic fibers became more radially aligned (Fig. 3A). This orthogonal alignment was also previously observed in the three cusps of the adult murine AoV[17,18].

At P0 there was no significant difference in the mean fluorescence intensity of AF633 in the leaflets of K5-Edn3 ($p = 0.7046$ $N = 3$, $n = 5$) and Albino mice ($p = 0.2175$ $N = 5$, $n = 13$) when compared to WT mice leaflets (Fig. 3B, left). At P7, leaflets of WT ($p = 0.0005$ $N = 3$, $n = 6$) and K5-Edn3 ($p < 0.0001$ $N = 3$, $n = 5$) mice had significantly increased mean fluorescence intensity of AF633 in comparison to that of Albino leaflets ($N = 5$, $n = 13$) (Fig. 3B, left). No significant differences were observed between the three groups for CNA35-488 mean fluorescent intensity at P0 and P7 stages (Fig. 3B, right). These results indicate that lack of leaflet pigmentation following peak postnatal *Eln* expression correlates with reduced formation of elastic fibers in AoV leaflets.

Both high and low levels of pigmentation alter *Eln* expression in AoV leaflets in neonatal stages

To determine if the differences in elastic fiber abundance in the AoV were due to changes in *Eln* expression, we performed RT-qPCR on AoV leaflets from the three mouse models. At P0, *Eln* expression was significantly ~ 12-fold higher in WT AoV when compared to K5-Edn3 ($p = 0.0002$) and Albino ($p = 0.0013$) AoVs. Interestingly, at P7 *Eln* expression trended higher in both K5-Edn3 ($p = 0.25$, ~ 7.66-fold change, $N = 6$) and Albino ($p = 0.90$, ~ 2.2-fold change, $N = 4$) compared WT leaflets (Fig. 3C), but the observed differences did not reach the established cutoff for statistical significance. Lastly, *Eln* expression was low at P30 in all three mouse models. These results suggest that both elevated and diminished levels of pigmentation in the leaflet affect *Eln* expression in early neonatal stages.

Alpha-smooth muscle actin and melanocytic marker positive cells express *Eln* during AoV development

Previous analyses could not identify a single population of *Eln* producing cells in the AoV; however, it was hypothesized that the lack of an observable population may have resulted from *Eln* production prior to the P7 timepoint considered[13]. Given our data that *Eln* expression peaks between P0-P5 (Fig. 1A), we analyzed the relationship between phenotypic markers and *Eln* at P0. Following the observed correlation between elastic fiber patterning and pigmentation, we first assessed the relationship between Eln, αSMA, and melanocytic markers.

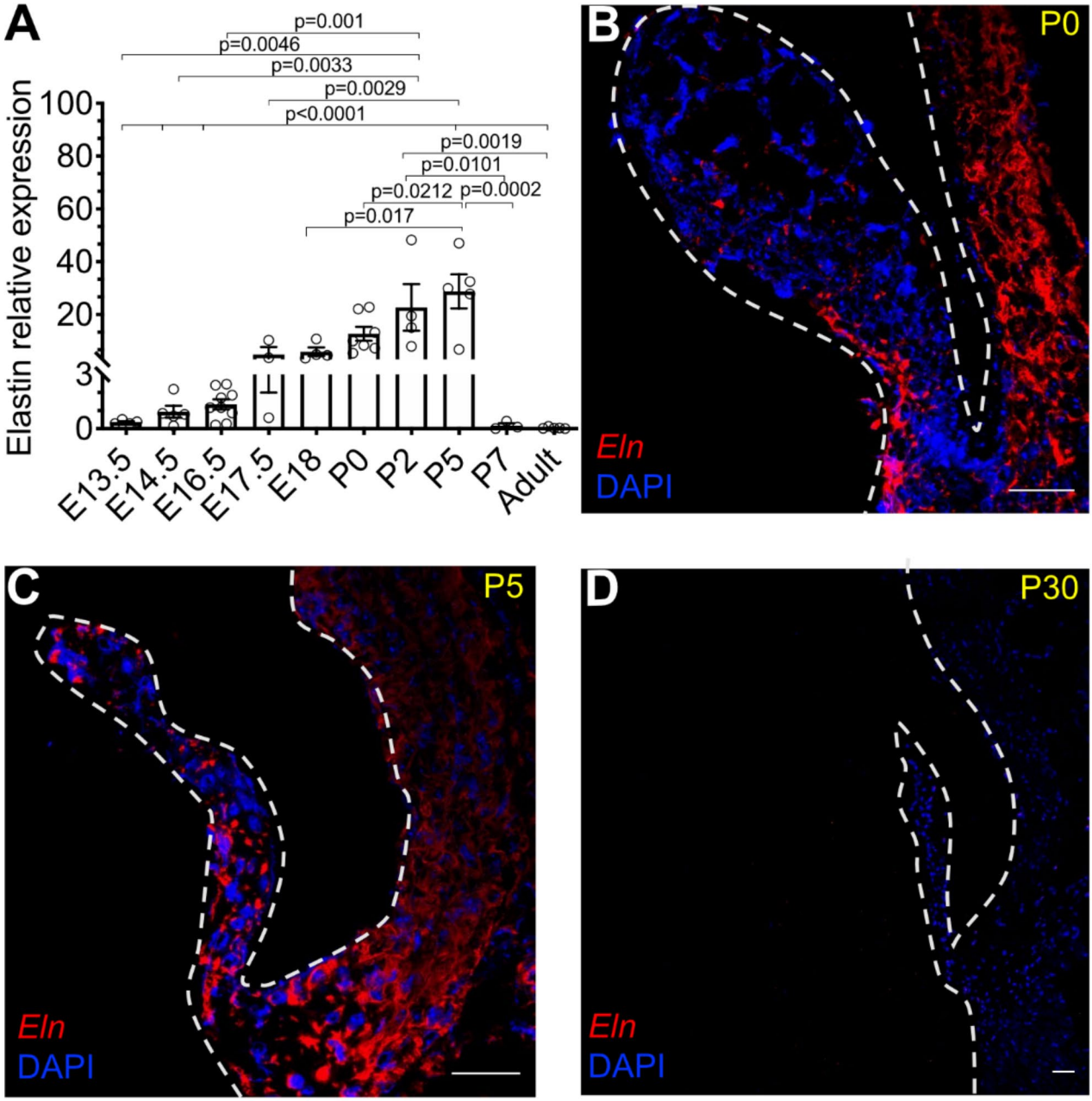

Fig. 1. ***Elastin***mRNA levels in developing murine aortic valve**.** (**A**) Timeline of *Eln* expression in AoV from early developmental stages to adulthood. qPCR fold change normalized to endogenous *Gapdh* gene. Mean ± SEM shown; $N = 5–9$ biological replicate per group; p-value determined by One-way ANOVA followed by Tukey's multiple comparison test. *In situ* hybridization RNAscope with *Eln* probe (red) and nuclei counterstaining for DAPI (blue) of (**B**) P0 (**C**) P5 (**D**) P30. Dotted white line outlines AoV leaflet. Scale bar = 10 μm.

Using *Tyr* and *Eln* RNAscope probes combined with immunolabeling for αSMA, we found a population of Eln^+ and $αSMA^+$ cells that express *Tyr* (Fig. 4A and B, Supplemental Fig. 3). Using immunolabeling, we next assessed other melanocytic markers, Trp1 and Mitf, (Fig. 4C and D) and found a population of $Trp1^+$ and $Mitf^+$ cells that are also Eln^+, substantiating our finding that AoV melanocytes can produce *Eln*.

Next, we assessed whether endothelial cells, which line the AoV surface, may contribute to elastogenesis. Using immunolabeling for VE-Cad, we observed a subset of VE-Cad positive cells to be Eln^+ (Fig. 5A). Next, we used Vimentin, which labels the majority of resident VICs and was used as a gene marker along with Col1a1, Col3a1 and Versican to cluster VICs in the previously mentioned single cell RNA Sequencing study[13]. We also observed a population of $Vimentin^+$ cells to be Eln^+ (Fig. 5B). Finally, using CD45 antibody to label local immune cells, we found these cells to be distinct from *Eln* expressing cells (Fig. 5C)**.** These findings suggest that several different cell phenotypes within the AoV can produce *Eln*.

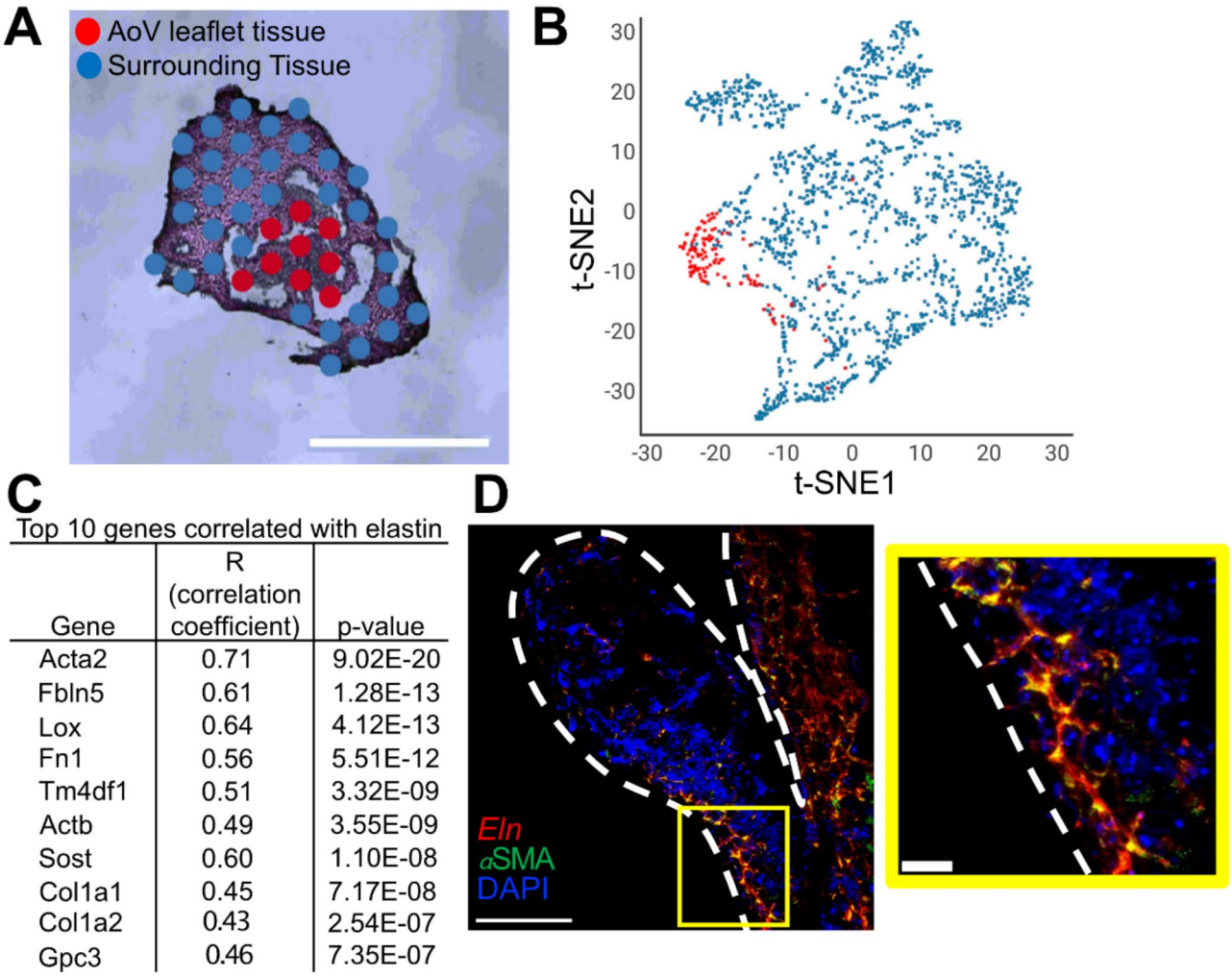

Gene	R (correlation coefficient)	p-value
Acta2	0.71	9.02E-20
Fbln5	0.61	1.28E-13
Lox	0.64	4.12E-13
Fn1	0.56	5.51E-12
Tm4df1	0.51	3.32E-09
Actb	0.49	3.55E-09
Sost	0.60	1.10E-08
Col1a1	0.45	7.17E-08
Col1a2	0.43	2.54E-07
Gpc3	0.46	7.35E-07

Fig. 2. Aortic valve cells clusters separately from other cardiac cells by spatial transcriptomic analysis at P3**.** (**A**) Spatial transcriptomics of P3 aortic valve sections. P3 aortic valve H&E image representation with surrounding tissue spots (blue) and aortic valve leaflet spots (red). Scale bar = 1 mm. (**B**) 2-D t-SNE cluster plot showing aortic valve leaflet tissue cluster (red) and surrounding tissue (blue). (**C**) List of top ten correlated genes with *Eln* from spatial transcriptomics data. For each spot (131 total), gene read count values were normalized to the total number of reads for a given spot. (**D**) *Eln* expressing cells are positive for alpha smooth muscle actin (αSMA). P0 aortic valve sections assessed by *in situ* hybridization RNAscope for *Eln* (red), immunofluorescence for αSMA antibody (green) and nuclei counterstaining for DAPI (blue). Dotted white line outlines aortic valve leaflet. Scale bar = 10 µm. Yellow highlighted box corresponds to the zoom image showing high magnification of αSMA and *Eln* positive cells in the aortic valve (left). Scalebar = 5 µm. $N = 6$.

Discussion

In this study, we established the timeline for *Eln* production and fiber deposition in the developing murine AoV. The timing of *Eln* production in the murine AoV corresponds to that reported for the human AoV. Elastogenesis peaks during the neonatal period and decreases considerably during adulthood in humans[31]. The fact that elastogenesis occurs during the same time in mice and humans indicates that our findings may have translational relevance. We further found that a portion of αSMA positive cells also express the common melanocytic marker, Tyr, and these double positive cells express *Eln*.

Cells expressing αSMA were previously reported to produce elastin in the lung[29] and blood vessels[30]. To our knowledge, this is the first time that a cell with a melanocytic phenotype (Tyr^{+}) is shown to directly express *Eln*. However, one previous report indicated that melanocyte precursors (Kit^{+}) in the murine embryonic skin express Eln binding protein and that Eln-derived peptide promotes melanogenesis by upregulating *Tyr* expression and dendrite formation[32], establishing a relationship between melanocytes and *Eln* in the skin. In Perivascular Epithelioid Cell (PEC) tumors, a population of cells expresses both melanocytic and myogenic markers including αSMA[33]. The cellular precursor of the PEC has not been established, but a possible NC origin has been suggested[34,35]. Another cell type that can co-express melanogenic genes such as *Tyr* and αSMA is the non-NC-derived pigment producing cell of the retinal pigment epithelium (RPE). RPE cells can be induced to

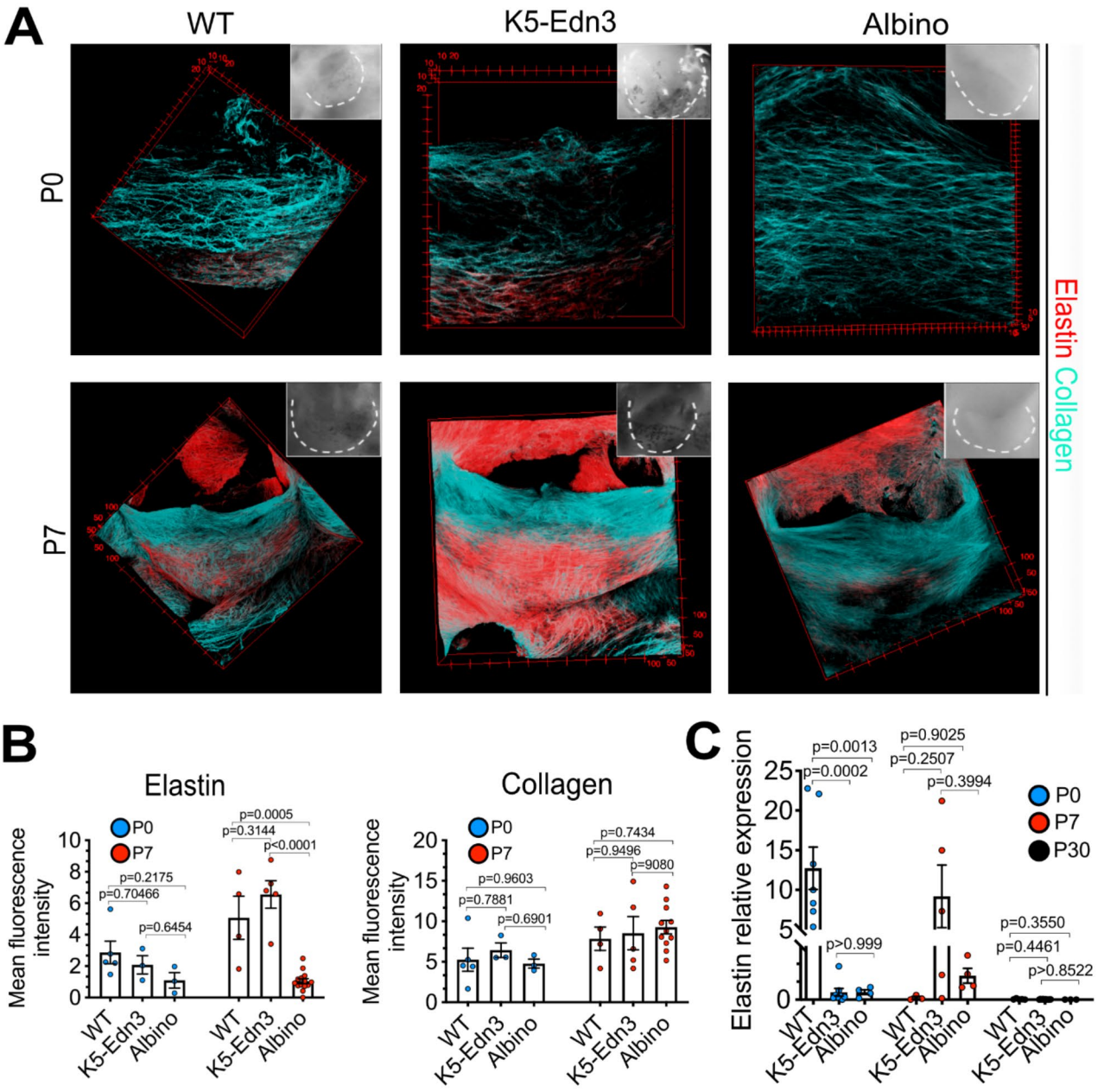

Fig. 3. Elastic fiber patterning in developing murine aortic valve. (**A**) Wholemount elastic (red) and collagen (cyan) fiber staining in WT (C57BL/6J mice), hyperpigmented (K5-Edn3) and hypopigmented (Albino) AoV leaflets at P0 and P7 stages. Leaflets in the light microscope images (inserts) correspond to those in the images of the stained leaflets. P0 images, 60X magnification and P7 images, 20X magnification. (**B**) Quantification of elastic fiber (left) and collagen fiber (right) staining at P0 (blue circle) and P7 (red circle) stages in WT, K5-Edn3 and Albino. (**C**) qPCR gene expression for elastin in K5-Edn3 and Albino at P0, P7 and P30 stages. P0 (blue circles), P7 (red circles) and P30 (black circles). Fold change normalized to endogenous *Gapdh*. Mean ± SEM shown; p-value determined by One-Way ANOVA followed by Tukey's multiple comparison test; $N = 5–9$ biological replicates per group.

express αSMA by Transforming Growth Factor beta (TGFβ)[35,36], a cytokine involved in normal development and pathological conditions of the AoV[37]. TGFβ is also a major positive regulator of elastogenesis acting at the transcriptional level, mediating tropoelastin mRNA stability and Eln degradation[38]. It is therefore plausible that in the developing murine AoV, TGFβ may be involved in modulating the fate of Eln producing cells. Another signaling pathway that may play an important role in the differentiation of Eln producing cells in the AoV is Wnt/β−catenin. When a constitutively active form of β−catenin is driven by the Tyr promoter during embryogenesis, a specific subpopulation of smooth muscle cells is replaced by melanocytes in the ductus arteriosus leading to improper closure suggesting that melanocyte competent precursor cells can acquire a smooth muscle cell fate[39].

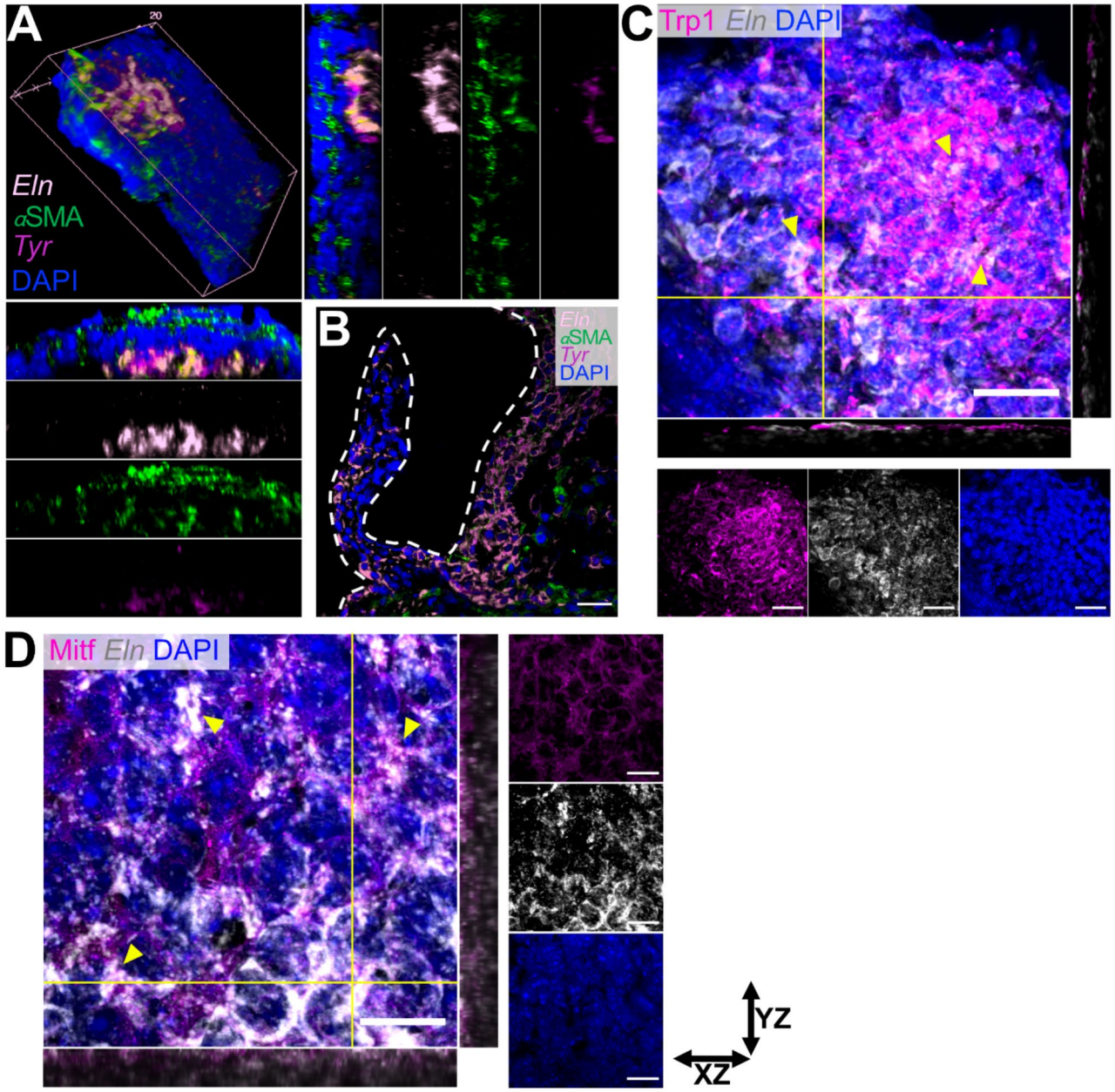

Fig. 4. Alpha smooth muscle actin expressing cells that are positive for melanocyte specific markers express ***elastin*** in aortic valve leaflets**.** (**A**) *Eln* expressing cells are positive for smooth muscle actin and melanocyte markers. 3-D reconstruction of P0 aortic valve wholemount leaflet labeled with elastin *(Eln, gray)* and Tyrosinase (*Tyr*, *magenta)* RNAscope probes, and alpha-smooth muscle actin (αSMA, green) immunolabeling. XZ and YZ orthogonal views for merged and separate channels are shown in the bottom and side panels, respectively. $N = 6$. (**B**) *In situ* hybridization with *Eln* and *Tyr* probe and immunofluorescence with αSMA immunolabeling of P0 aortic valve section. Dotted white line outlines aortic valve leaflet. Scale bar = 10 µm. $N = 4$. *In situ* hybridization of wholemount P3 WT aortic valve labeled for *Eln* (gray) and antibody staining (magenta) for (**C**) Tyrosine related protein 1 (Trp1), (**D**) Microphthalmia-associated transcription factor (Mitf) and nuclei counterstaining for DAPI (blue). Scale bar = 50 µm. Yellow arrow heads point to markers co-localization. The yellow line shows the cross section corresponding to the orthogonal views. The XZ and YZ orthogonal views are shown in the bottom and side panels with only magenta and gray channel, respectively. $N = 6$. Wholemount single channels images are shown for each of the corresponding marker.

We also observed a population of *Eln* producing cells that did not express αSMA and *Tyr*, further suggesting that elastogenesis is regulated by multiple cell types. Combining *in situ* hybridization and immunofluorescence, we found that *Eln* is produced in endothelial cells, VICs, but not by resident immune cells labeled with CD45. In the developing lung, pleural mesothelial cells, airway epithelial cells, and endothelial cells have also been shown to produce *Eln*[4]. Our spatial transcriptomic data showed high correlations between *Eln* and Acta2, Col1a1,

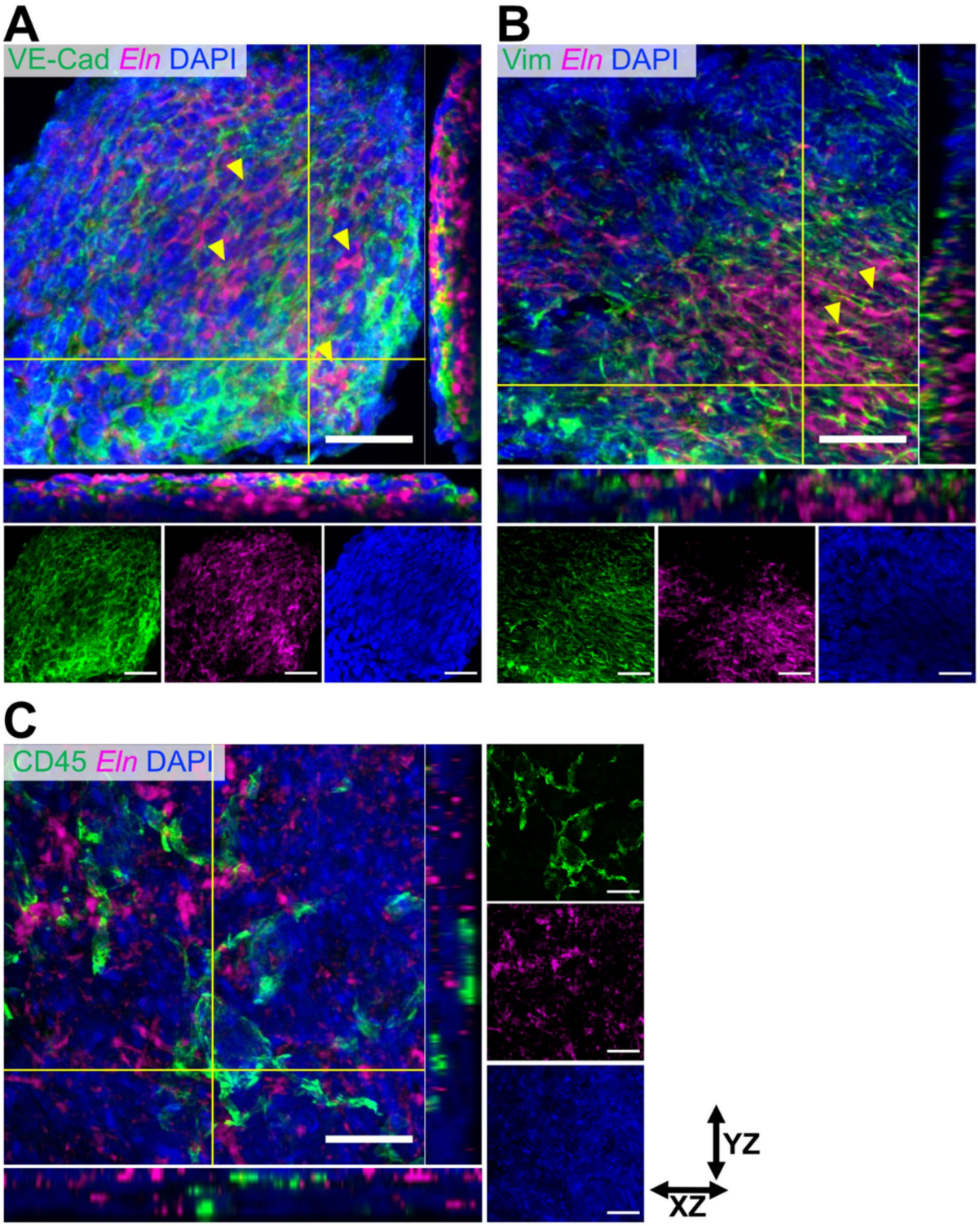

Fig. 5. Endothelial and interstitial cells express elastin mRNA except immune cells**.** 3-D reconstruction of P3 WT aortic valve wholemount leaflet labeled for elastin *(Eln*, *magenta) in situ* hybridization RNAscope probe, and antibody staining (green) for (**A**) VE-Cadherin (VE-Cad), (**B**) Vimentin (Vim), (**C**) CD45 and nuclei counterstaining for DAPI (blue). Yellow arrow heads points to co-localization. The yellow line shows the cross section corresponding to the orthogonal views. The XZ and YZ orthogonal views are shown in the bottom and side panels with only magenta and gray channel, respectively. $N = 6$. Scale bar = 50 µm. Wholemount single channels images are shown for each of the corresponding marker.

Col1a2, Col4a1, and Actb, which are markers abundantly present in the AoV. We also found Fbln5 and Lox to be highly correlated with Eln, which are known mediators of elastogenesis in the aorta. Spatial transcriptomics provides powerful spatial information and overcomes the challenges with cell dissociation in single cell RNA-Seq, yet the technique does not generate single cell resolution nor high transcript coverage data, which may have masked contributions from lower abundance cells (e.g., melanocytes) in the correlations.

We have previously shown a relation between elastic fiber patterning and pigment presence in the murine AoV[17,18]. Thus, we further explored the patterning of elastic fibers during early postnatal development with the variation of pigment. The initial pattern of elastic fibers in the hyperpigmented AoV of K5-Edn3 mice at P0 is disorganized and remain as such into adulthood and one of its consequences may be the observed delay in the peak of *Eln* expression at P7. Perhaps, in hyperpigmented valves, *Eln* is still transcriptionally regulated in late postnatal development to compensate for the disorganization in Eln fiber production. As in the adult hypopigmented albino AoV, P0 leaflets are also devoid of elastic fibers and the peak of *Eln* expression is both delayed and considerably decreased when compared to the WT AoV. Interestingly, hypopigmented areas in the skin of human vitiligo patients, have less melanocytes and elastic fibers, but not collagen, corroborating the association between pigmentation and Eln fiber patterning[40,41]. This association could be attributed to fiber stability and, thus, the slight delayed peak of *Eln* expression observed in the albino AoV may result in the instability of the Eln fibers. Regardless, these findings suggest a strong correlation between pigmentation and the elastic fiber patterning in the mouse AoV during early postnatal development. Moreover, although *Eln* is produced in mutants, gene expression delay or lower expression levels may be a key factor affecting the adult patterning. Future studies should investigate other factors responsible for the phenotype such as proteoglycans and other key components that are crucial for the stability of fiber alignment. Deficiency in Emilin 1, an Eln binding protein, results in elastic fiber fragmentation and increase stiffness prior to onset of fibrosis[42]. Other factors such as mechanical forces may also affect elastic fiber patterning[17]. Future studies will assess the role of mechanics and other factors involved in elastogenesis in the observed phenotypes. Furthermore, future studies should also consider tracking left, right and non-coronary leaflets as they receive contributions from different developmental precursors[14].

Since pigmentation has not been described in the human AoV, a potential contribution of melanocyte-like cells to human valve function and homeostasis have not been explored. We have previously shown that DCT^+ cells are present in the human AoV adjacent to endothelial cells on the ventricular aspect of aortic valve leaflets[18]. A recent study identified a population of human fetal VICs associated with elastic fiber formation in a similar localization in the leaflet[43]. Furthermore, other pigmentation related markers (TRP1, MART1) have been detected in the human AoV[44] . We also observed a persistence of markers critical for melanogenesis, such as *Dct*, *Trp1*, *Tyr*, and *Mitf* from E13.5 into adulthood in the mouse AoV (Supplemental Fig. 4, Supplemental Table S1). Thus, cells with a melanocyte like phenotype are present in the murine AoV and could be involved in human AoV elastogenesis. Previous transcriptomic analyses of single cells from murine P7 and P30 AoVs showed a distinct subset of melanocytes along with other known populations such as endothelial, immune, and VICs[13], further substantiating our findings that $Trp1^+$ and Tyr^+ cells are present in the developing AoV. The transcriptomic study did not identify a population of *Eln* producing cells, most likely because of technical issues related to the number of cells used for sequencing or because P7 may have already been too late to allow for detection of *Eln* as per our *Eln* expression timeline.

For future studies, lineage tracing experiments using the appropriate driven Cre systems (i.e., Tie2, Wnt1, Nkx2.5, Isl1, Mef2c) should be carried out to unravel the origin of the various cells observed in the mature AoV. Single cell transcriptomic or spatial transcriptomics studies at various stages of pre- and postnatal development will also help establish if VICs derived from each of the contributing lineages have different functions in valve maturation and homeostasis particularly in the context of elastogenesis. Although pigmentation has not been reported in human AoV leaflets, no analyses have been carried out with fetal valves. Since elastin expression is highest at these developmental stages, fetal valves should be examined for the presence of pigmentation and melanocytic markers.

Data availability

All the spatial transcriptomics datasets generated and analyzed during this current study are available in the Gene Expression Omnibus (GEO) database with Accession Number GSE254500.

Received: 4 January 2024; Accepted: 19 September 2024
Published online: 26 October 2024

References

1. Aikawa, E. et al. Human semilunar cardiac valve remodeling by activated cells from fetus to adult: implications for postnatal adaptation, pathology, and tissue engineering. *Circulation*. **113**, 1344–1352. https://doi.org/10.1161/CIRCULATIONAHA.105.591768 (2006).
2. Weihermann, A. C., Lorencini, M., Brohem, C. A. & de Carvalho, C. M. Elastin structure and its involvement in skin photoageing. *Int. J. Cosmet. Sci.***39**, 241–247. https://doi.org/10.1111/ics.12372 (2017).
3. Vindin, H. J., Oliver, B. G. & Weiss, A. S. Elastin in healthy and diseased lung. *Curr. Opin. Biotechnol.***74**, 15–20. https://doi.org/10.1016/j.copbio.2021.10.025 (2022).
4. Mecham, R. P. Elastin in lung development and disease pathogenesis. *Matrix Biol.***73**, 6–20. https://doi.org/10.1016/j.matbio.2018.01.005 (2018).
5. McLean, S. E., Mecham, B. H., Kelleher, C. M., Mariani, T. J., & Mecham, R. P. (2005). Extracellular matrix gene expression in the developing mouse aorta. In J. Miner (Ed.), *Extracellular Matrix in Development and Disease* (pp. 81-128). (Advances in Developmental Biology; Vol. 15). https://doi.org/10.1016/S1574-3349%2805%2915003-0
6. Vrhovski, B. & Weiss, A. S. Biochemistry of tropoelastin. *Eur. J. Biochem.***258**, 1–18. https://doi.org/10.1046/j.1432-1327.1998.2580001.x (1998).

7. Schenke-Layland, K. et al. Comparative study of cellular and extracellular matrix composition of native and tissue engineered heart valves. *Matrix Biol.***23**, 113–125. https://doi.org/10.1016/j.matbio.2004.03.005 (2004).
8. Le, V. P., Knutsen, R. H., Mecham, R. P. & Wagenseil, J. E. Decreased aortic diameter and compliance precedes blood pressure increases in postnatal development of elastin-insufficient mice. *Am. J. Physiol. Heart Circ. Physiol.***301**, H221–229. https://doi.org/10.1152/ajpheart.00119.2011 (2011).
9. Li, D. Y. et al. Elastin is an essential determinant of arterial morphogenesis. *Nature*. **393**, 276–280. https://doi.org/10.1038/30522 (1998).
10. Hinton, R. B. et al. Elastin haploinsufficiency results in progressive aortic valve malformation and latent valve disease in a mouse model. *Circ. Res.***107**, 549–557. https://doi.org/10.1161/CIRCRESAHA.110.221358 (2010).
11. Longobardo, L. et al. Impairment of elastic properties of the aorta in bicuspid aortic valve: relationship between biomolecular and aortic strain patterns. *Eur. Heart J. Cardiovasc. Imaging*. **19**, 879–887. https://doi.org/10.1093/ehjci/jex224 (2018).
12. Perrotta, I. et al. New evidence for a critical role of elastin in calcification of native heart valves: immunohistochemical and ultrastructural study with literature review. *Histopathology*. **59**, 504–513. https://doi.org/10.1111/j.1365-2559.2011.03977.x (2011).
13. Hulin, A. et al. Maturation of heart valve cell populations during postnatal remodeling. *Development*. **146**https://doi.org/10.1242/dev.173047 (2019).
14. Eley, L. et al. A novel source of arterial valve cells linked to bicuspid aortic valve without raphe in mice. *Elife*. **7**https://doi.org/10.7554/eLife.34110 (2018).
15. Peterson, J. C. et al. Bicuspid aortic valve formation: Nos3 mutation leads to abnormal lineage patterning of neural crest cells and the second heart field. *Dis. Model. Mech.***11**https://doi.org/10.1242/dmm.034637 (2018).
16. Brito, F. C. & Kos, L. Timeline and distribution of melanocyte precursors in the mouse heart. *Pigment Cell. Melanoma Res.***21**, 464–470. https://doi.org/10.1111/j.1755-148X.2008.00459.x (2008).
17. Nasim, S. et al. Pigmentation affects Elastic Fiber Patterning and Biomechanical Behavior of the murine aortic valve. *Front. Cardiovasc. Med.***8**, 754560. https://doi.org/10.3389/fcvm.2021.754560 (2021).
18. Hutcheson, J. D. et al. Elastogenesis correlates with pigment production in murine aortic valve leaflets. *Front. Cardiovasc. Med.***8**, 678401. https://doi.org/10.3389/fcvm.2021.678401 (2021).
19. Garcia, R. J. et al. Endothelin 3 induces skin pigmentation in a keratin-driven inducible mouse model. *J. Invest. Dermatol.***128**, 131–142. https://doi.org/10.1038/sj.jid.5700948 (2008).
20. Clifford, P. S. et al. Spatial distribution and mechanical function of elastin in resistance arteries: a role in bearing longitudinal stress. *Arterioscler. Thromb. Vasc Biol.***31**, 2889–2896. https://doi.org/10.1161/ATVBAHA.111.236570 (2011).
21. Shen, Z., Lu, Z., Chhatbar, P. Y., O'Herron, P. & Kara, P. An artery-specific fluorescent dye for studying neurovascular coupling. *Nat. Methods*. **9**, 273–276. https://doi.org/10.1038/nmeth.1857 (2012).
22. Aper, S. J. et al. Colorful protein-based fluorescent probes for collagen imaging. *PLoS One*. **9**, e114983. https://doi.org/10.1371/journal.pone.0114983 (2014).
23. Schindelin, J. et al. Fiji: an open-source platform for biological-image analysis. *Nat. Methods*. **9**, 676–682. https://doi.org/10.1038/nmeth.2019 (2012).
24. Akoglu, H. User's guide to correlation coefficients. *Turk. J. Emerg. Med.***18**, 91–93. https://doi.org/10.1016/j.tjem.2018.08.001 (2018).
25. Chan, Y. H. Biostatistics 104: correlational analysis. *Singap. Med. J.***44**, 614–619 (2003).
26. Choi, J. et al. Analysis of dermal elastic fibers in the absence of fibulin-5 reveals potential roles for fibulin-5 in elastic fiber assembly. *Matrix Biol.***28**, 211–220. https://doi.org/10.1016/j.matbio.2009.03.004 (2009).
27. Brown-Augsburger, P., Tisdale, C., Broekelmann, T., Sloan, C. & Mecham, R. P. Identification of an elastin cross-linking domain that joins three peptide chains. Possible role in nucleated assembly. *J. Biol. Chem.***270**, 17778–17783. https://doi.org/10.1074/jbc.270.30.17778 (1995).
28. Narayanan, A. S., Page, R. C., Kuzan, F. & Cooper, C. G. Elastin cross-linking in vitro. Studies on factors influencing the formation of desmosines by lysyl oxidase action on tropoelastin. *Biochem. J.***173**, 857–862. https://doi.org/10.1042/bj1730857 (1978).
29. Liu, S., Parameswaran, H., Young, S. M. & Varisco, B. M. JNK suppresses pulmonary fibroblast elastogenesis during alveolar development. *Respir Res.***15**, 34. https://doi.org/10.1186/1465-9921-15-34 (2014).
30. Lin, C. J. et al. Heterogeneous Cellular contributions to Elastic Laminae formation in arterial Wall Development. *Circ. Res.***125**, 1006–1018. https://doi.org/10.1161/CIRCRESAHA.119.315348 (2019).
31. Votteler, M. et al. Elastogenesis at the onset of human cardiac valve development. *Development*. **140**, 2345–2353. https://doi.org/10.1242/dev.093500 (2013).
32. Chang, C. H. et al. Melanocyte precursors express elastin binding protein and elastin-derived peptide (VGVAPG) stimulates their melanogenesis and dendrite formation. *J. Dermatol. Sci.***51**, 158–170. https://doi.org/10.1016/j.jdermsci.2008.03.010 (2008).
33. Utpatel, K. et al. Complexity of PEComas: diagnostic approach, molecular background, clinical management. *Pathologe*. **41**, 9–19. https://doi.org/10.1007/s00292-019-0612-5 (2020).
34. Fernandez-Flores, A. Evidence on the neural crest origin of PEComas. *Rom J. Morphol. Embryol.***52**, 7–13 (2011).
35. Stocks, S. Z., Taylor, S. M. & Shiels, I. A. Transforming growth factor-beta1 induces alpha-smooth muscle actin expression and fibronectin synthesis in cultured human retinal pigment epithelial cells. *Clin. Exp. Ophthalmol.***29**, 33–37. https://doi.org/10.1046/j.1442-9071.2001.00368.x (2001).
36. Kurosaka, D., Muraki, Y., Inoue, M. & Katsura, H. TGF-beta 2 increases alpha-smooth muscle actin expression in bovine retinal pigment epithelial cells. *Curr. Eye Res.***15**, 1144–1147. https://doi.org/10.3109/02713689608995147 (1996).
37. Menon, V. & Lincoln, J. The genetic regulation of aortic Valve Development and Calcific Disease. *Front. Cardiovasc. Med.***5**, 162. https://doi.org/10.3389/fcvm.2018.00162 (2018).
38. Sproul, E. P. & Argraves, W. S. A cytokine axis regulates elastin formation and degradation. *Matrix Biol.***32**, 86–94. https://doi.org/10.1016/j.matbio.2012.11.004 (2013).
39. Yajima, I. et al. A subpopulation of smooth muscle cells, derived from melanocyte-competent precursors, prevents patent ductus arteriosus. *PLoS One*. **8**, e53183. https://doi.org/10.1371/journal.pone.0053183 (2013).
40. Hirobe, T., Enami, H. & Nakayama, A. Elastin fiber but not collagen fiber is decreased dramatically in the dermis of vitiligo patients. *Int. J. Dermatol.***59**, e369–e372. https://doi.org/10.1111/ijd.14896 (2020).
41. Hirobe, T. & Enami, H. Reduced elastin fibers and melanocyte loss in Vitiliginous skin are restored after repigmentation by Phototherapy and/or autologous minigraft transplantation. *Int. J. Mol. Sci.***23**https://doi.org/10.3390/ijms232315361 (2022).
42. Angel, P. M. et al. Proteomic Alterations Associated with Biomechanical Dysfunction are early processes in the Emilin1 deficient mouse model of aortic valve disease. *Ann. Biomed. Eng.***45**, 2548–2562. https://doi.org/10.1007/s10439-017-1899-0 (2017).
43. Liu, Z. et al. APOE–NOTCH axis governs elastogenesis during human cardiac valve remodeling. *Nat. Cardiovasc. Res.*https://doi.org/10.1038/s44161-024-00510-3 (2024).
44. Gottlieb Sen, D. et al. The Transcriptional signature of growth in human fetal aortic Valve Development. *Ann. Thorac. Surg.***106**, 1834–1840. https://doi.org/10.1016/j.athoracsur.2018.06.034 (2018).

Acknowledgements

We would like to thank the FIU Confocal Core Facility and the University of Florida ICBR Next Gen DNA Sequencing Core. Data analysis was performed in part by the University of Florida ICBR Bioinformatics Core

Facility, RRID: SCR_019120. We would also like to thank Jorge Rubinos for maintaining mouse colonies.

Author contributions

S.N designed the experiments, drafted the manuscript, conducted the aortic valve dissections, staining, confocal imaging, and data analysis. B.A.A. dissected the embryos and isolated the aortic valves for elastin timeline. D.C. dissected and sectioned P3 mouse aortic valves, imaged slides for spatial transcriptomics, and performed spatial transcriptomic analyses. P.S.N. performed spatial transcriptomics, RNAscope wholemount staining and imaging of P3 aortic valves. A.R. performed quality control and initial analysis on the spatial transcriptomics data. L.K and J.D.H equally designed the experiments, supervised S.N, and reviewed all the versions of the manuscript. All authors read and approved the final manuscript.

Funding

This work was supported by the Florida Heart Research Foundation. S.N. was partially funded by Florida International University Graduate School. D.C. and P.S.N. are supported by the Florida Heart Research Foundation Doctoral Student Grant.

Declarations

Competing interests

The authors declare no competing interests.

Additional information

Supplementary Information The online version contains supplementary material available at https://doi.org/10.1038/s41598-024-73673-5.

Correspondence and requests for materials should be addressed to J.D.H. or L.K.